 CMES, vol.61, no.1, pp.1-22, 2010

Application of Energy Finite Element Method to High-frequency Structural-acoustic Coupling of an Aircraft Cabin with Truncated Conical Shape

M. X. Xie[1], H. L. Chen[1], J. H. Wu[1] and F. G. Sun[1]

Abstract: Energy finite element method (EFEM) is a new method to solve high-frequency structural-acoustic coupling problems, but its use has been limited to solving simple structures such as rods, beams, plates and combined structures. In this paper, the high-frequency structural-acoustic coupling characteristics of an aircraft cabin are simulated by regarding the shell as a number of flat shell elements connected with a certain angle in EFEM. Two tests validated the method employed in this paper. First, the structural response analysis of a cylinder was calculated in two ways: dividing the shell by axis-symmetric shells after deriving the governing equation of axis-symmetric vibration; and using flat shell elements to approximate the shell structure, as proposed by this paper. The second verification used an EFEM analysis of a simple passenger vehicle and compared the analysis with results reported in literature. Comparison between results in both tests produced good correlation. With the method validated, the structural-acoustic coupling characteristics of an aircraft cabin with two end plates were investigated. A wind tunnel test provided the fluctuating pressure load imposed on the exterior of a truncated conical aircraft cabin, and the structural-acoustic coupling characteristics of the aircraft cabin with two end plates have been investigated with the verified method. The detailed distribution of the flexural energies on the cabin surface and the distribution of acoustic pressures in the inner space of the cabin under the coupling condition were then obtained using the new method.

Keywords: energy finite element method, structural-acoustic coupling, aircraft cabin.

[1] Institute of Vibration and Noise Control, School of Mechanical Engineering, Xi'an Jiaotong University, Xi'an 710049, P.R. China

1 Introduction

Structural-acoustic coupling problems have been experiencing growing interest from scientists and engineers for some time. Much research has been done to precisely predict the structural-acoustic response and design structures necessary for best acoustical comfort and least vibrational destruction. For structural-acoustic coupling response, a great number of numerical studies have been performed using finite element method (FEM) and boundary element method (BEM) [Brancati A., Aliabadi M. H., Benedetti I. (2009)]. However, FEM and BEM are not always efficient and accurate, especially for high frequency ranges, since structural response is extremely sensitive to material and geometry details [Bitsie F. (1996)]. In order to capture the structural characteristic length in high frequency ranges, a much smaller mesh size is necessary for FEM or BEM models, which results in the procedure being computationally expensive or even prohibitive. Statistical energy analysis (SEA) is an alternative efficient method which is suitable for solving high-frequency problems and has been widely used as an analysis tool in practice. But local modeling details that concern designers are usually ignored in SEA due to the fact that SEA is based on the division of sub-structures.

The energy finite element method (EFEM) presented by Nefske *et al* [Nefske D. J., Sung S. H. (1989)] is a new tool for structural-acoustic coupling analysis. In this method, governing differential equations are derived in terms of energy density variables which are solved by applying the finite element approach. Significant advances have been made with the aid of EFEM [Bernhard R. J., Huff J. E. (1999); Zhang W.G. (2003); Moravaeji S.J. (2008); Yan X. Y. (2008)], including solutions to many high-frequency structural-acoustic problems. Bitsie presented coupling relationships between structural and acoustic domains based on the definition of radiation efficiency [Bitsie F. (1996)]. Zhang *et al* [Zhang W.G., Wang A.M., Vlahopoulos N. (2002)] derived the governing differential equations of energy density by considering the acoustic or the flexural response as a summation of incoherent orthogonal waves. In their study, the orthogonal waves constitute a basis for expressing the behavior of the plate or the acoustic space and a vessel that is comprised by both acoustic spaces and structural components was analyzed. Wu and Vlahopoulos summarized the development of EFEM, concluding that EFEM comprises a general purpose simulation method for vibration and acoustic analysis of complex systems [Wu K.C., Vlahopoulos N. (2004); Wu K.C., Vlahopoulos N. (2006)]. Raymond *et al.* compared the computational cost of EFEM with respect to SEA for acoustic modeling and indicated that EFEM was potentially applicable for detailed analysis of the acoustic environment and the response of surface ships to various excitation sources [Raymond F., Leo B.,Layton G., David B. (2006)]. Zhang and Raveendra discussed the unique benefits of EFEM through investiga-

tion of several example problems [Zhang W. G., Raveendra S.T. (2008)]. EFEM is one of the best choices for solving high-frequency structural-acoustic problems owing to its flexibility and accuracy.

Among EFEM investigation objects, however, little work has been done on shell structures possessing a complicated geometry. The primary basis of EFEM is deriving the governing differential equations in terms of energy density variables and then employing a finite element approach to solving those equations numerically. However, deriving energy density governing equations of a general shell, such as the truncated conical cabin studied in this work, is not easy [Steffen Marburg, Bodo Nolte, Robert Bernhard, Shuo Wang. (2008)]. But in many engineering fields, such as aviation and spaceflight, structural systems combined by shell structures are unavoidable.

This paper develops an approximate approach that regards a shell structure as a number of flat shell elements connected at specific angles to simulate, with EFEM, the coupling behavior of a shell structural-acoustic system at high frequencies. The accuracy of this method is first verified with a cylindrical shell, which possess a simple geometry and for which the derivation of the energy density governing equation is relatively easy. Then the high-frequency structural-acoustic coupling characteristics of an aircraft cabin shell structure with a truncated conical shape are calculated by this method. Furthermore, the fluctuating pressure loads which are imposed on the exterior of an aircraft cabin with a truncated conical shape are obtained through a wind tunnel test. Finally, the distribution of flexural energies on the surface of the aircraft cabin and the distribution of acoustic pressures in its inner space under the high-frequency coupling condition are obtained with the aid of the verified method.

2 Introduction of the approximate method for shell structures in EFEM

A complex structural-acoustic system is comprised of structural and acoustic spaces, where structure can take the form of bar, beam, plate or shell. There are two processes in EFEM: deriving governing differential equations in terms of energy density variables, and employing a finite element approach for solving those equations numerically. The governing differential equations of energy density for bar, beam and plate have already been derived and reported by many researchers, but little literature is available for the energy density governing equations for general shell structures [Steffen Marburg, Bodo Nolte, Robert Bernhard, Shuo Wang. (2008)]. The authors of this paper derived the energy density equations of a cylinder in their previous works, but they were limited to axis-symmetric loads. To solve the high-frequency structural-acoustic problem of a shell structure with truncated conical shape with EFEM in this work, the shell is divided into flat shell elements for which

the governing differential equations of plates is available. Furthermore, the power transfer coefficients between adjacent elements were calculated by the dynamic stiffness matrix method, the governing differential equations of acoustic space, and the relationship between the structure and acoustic spaces were developed. Finally, structural-acoustic coupling problems of a complex system containing shells were solved using EFEM.

For the structural-acoustic coupling problem of a complex system, the structural-acoustic effect needs to be considered. The governing equations are written as [Bitsie F. (1996); Bouthier O. M.; Bernhard R. J. (1995)]

$$\begin{aligned}
&-\frac{C_{gB}^2}{(\eta_{sB}+\eta_{rad})\,\omega}\nabla^2\langle\bar{e}_{sB}\rangle+(\eta_{sB}+\eta_{rad})\,\omega\langle\bar{e}_{sB}\rangle=\langle\bar{\pi}_{sB}\rangle\\
&-\frac{C_{gL}^2}{\eta_{sL}\omega}\nabla^2\langle\bar{e}_{sL}\rangle+\eta_{sL}\omega\langle\bar{e}_{sL}\rangle=\langle\bar{\pi}_{sL}\rangle\\
&-\frac{C_{gT}^2}{\eta_{sT}\omega}\nabla^2\langle\bar{e}_{sT}\rangle+\eta_{sT}\omega\langle\bar{e}_{sT}\rangle=\langle\bar{\pi}_{sT}\rangle\\
&-\frac{c_a^2}{\eta_a\omega}\nabla^2\langle\bar{e}_a\rangle+\eta_a\omega\langle\bar{e}_a\rangle=\langle\bar{\pi}_a\rangle
\end{aligned}\tag{1}$$

where: C is the wave speed; subscripts B, L and T express the respective bending, longitudinal and transverse shear waves; subscript g means group speed; subscripts s and a are used to denote structure and acoustic domains; η is the damping loss factor; η_{rad} is the radiation damping; ω is the radian frequency of the harmonic excitation; $\langle\bar{e}\rangle$ is the time average over a period and space average over a wavelength of energy density; and $\langle\bar{\pi}\rangle$ is the time average over a period and space average over a wavelength of input power density.

Using the Galerkin weighted residual scheme and the Lagrangian shape function

as the trial function, Equation (1) can be rewritten as

$$\begin{aligned}
&\sum_{j=1}^{n}\int_{\Omega_{si}}\left[\frac{C_{gB}^2}{(\eta_{sB}+\eta_{rad})\,\omega}\nabla\phi_i\nabla\phi_j+(\eta_{sB}+\eta_{rad})\,\omega\phi_i\phi_j dxdy\right]e_j\\
&-\int_{\Omega_{si}}\phi_i\pi_{in}dxdy-\int_{\Gamma_{si}}\phi_i q d\Gamma_{si}=0\\
&\sum_{j=1}^{n}\int_{\Omega_{si}}\left[\frac{C_{gL}^2}{\eta_{sL}\omega}\nabla\phi_i\nabla\phi_j+\eta_{sL}\omega\phi_i\phi_j dxdy\right]e_j-\int_{\Omega_{si}}\phi_i\pi_{in}dxdy-\int_{\Gamma_{si}}\phi_i q d\Gamma_{si}=0\\
&\sum_{j=1}^{n}\int_{\Omega_{si}}\left[\frac{C_{gT}^2}{\eta_{sT}\omega}\nabla\phi_i\nabla\phi_j+\eta_{sT}\omega\phi_i\phi_j dxdy\right]e_j-\int_{\Omega_{si}}\phi_i\pi_{in}dxdy-\int_{\Gamma_{si}}\phi_i q d\Gamma_{si}=0\\
&\sum_{j=1}^{n}\int_{\Omega_{ai}}\left[\frac{c_a^2}{\eta_a\omega}\nabla\phi_i\nabla\phi_j+\eta_a\omega\phi_i\phi_j dxdy\right]e_j-\int_{\Omega_{ai}}\phi_i\pi_{in}dxdy-\int_{\Gamma_{ai}}\phi_i q d\Gamma_{ai}=0
\end{aligned}\tag{2}$$

Here Γ_{si} is the element boundary, Ω_{si} is the area domain of the element, e_j is the time and space average energy density of node j, ϕ_j is the Lagrange interpolating function, q is energy flow, $q=-c_g^2\eta\,\omega\nabla e\cdot\vec{n}$, and $\vec{n}$ is the unit normal vector of the boundary.

At a structural-structural junction, the structural waves will be transmitted and reflected. Adjacent structural panels have different energy densities at the junction, but the power flow for adjacent panels remains continuous at the junction [Bouthier O. M.; Bernhard R. J. (1995)]. The relationship between the net power flow and the energy density on the different sides of a junction can be expressed as

$$\begin{Bmatrix} q_B^i\\ q_L^i\\ q_T^i\\ q_B^j\\ q_L^j\\ q_T^j\end{Bmatrix}=(I_{ss}-\tau_{ss})\,(I_{ss}+\tau_{ss})^{-1}\begin{bmatrix} c_{gB}^i & 0 & 0 & 0 & 0 & 0\\ 0 & c_{gL}^i & 0 & 0 & 0 & 0\\ 0 & 0 & c_{gT}^i & 0 & 0 & 0\\ 0 & 0 & 0 & c_{gB}^j & 0 & 0\\ 0 & 0 & 0 & 0 & c_{gL}^j & 0\\ 0 & 0 & 0 & 0 & 0 & c_{gT}^j\end{bmatrix}\begin{Bmatrix} e_B^i\\ e_L^i\\ e_T^i\\ e_B^j\\ e_L^j\\ e_T^j\end{Bmatrix}\tag{3}$$

where: q is power flow; I is the identity matrix; τ are power transfer coefficients which can be calculated using a dynamic stiffness matrix method for elastic wave transmission developed by Langley and Heron [Langley R.S., Heron K.H. (1990)]; c is structural wave speed; e is energy density; subscripts B, L, T are the bending, longitudinal and transverse shear waves, respectively; subscript g denotes group speed; and superscripts i and j are for the structural i and j at the junction. Through

Equation (3), the energy density e of structural i and j at the junction is estimated by power flow q. The coupling energy forms are expressed explicitly in terms of the energy density variables. When dividing the shell by the flat shell element, it is necessary to compute the power transfer coefficients between the adjacent flat shell elements. The power transfer coefficients are computed by means of the dynamic stiffness matrix method.

At the interface between structure and acoustic space, the bending wave will transmit into the acoustic space and interact with the acoustic wave. For a lossless structural-acoustic joint, the net power flow at the structural-acoustic joint and the energy density on both sides of the structural-acoustic interface can be written as

$$\begin{Bmatrix} q_{sB} \\ q_a \end{Bmatrix} = (I_{sa} - \tau_{sa})(I_{sa} + \tau_{sa})^{-1} \begin{bmatrix} c_{gB} & 0 \\ 0 & c_a \end{bmatrix} \begin{Bmatrix} e_{sB} \\ e_a \end{Bmatrix} \tag{4}$$

By substituting Equations (3) and (4) into Equation (2), Equation (2) is comprised of only variable e. Therefore, we can solve the equation numerically to obtain e on every node of the structural-acoustic system.

3 Verification of the approximate method in EFEM

Because the governing equation of a cylinder is easy to derive, a cylinder model is used to validate the flat shell element model introduced in the previous section. Comparison of dynamic response results of the cylindrical shell was performed by two methods.

For the first case, we derive the governing equation for the cylindrical shell by taking advantage of the simple shape and then divide the simple shell by its shell element to calculate the dynamic response of the shell. The same cylindrical shell is then computed using the approximate method introduced in the previous section.

For the axis-symmetric deformation of a cylindrical shell, the motion equation is expressed as [He F.B., Shen Y.P. (2008)]

$$D(1+i\eta)\frac{d^4w}{dx^4} + \frac{Eh}{a^2}w + \rho h\frac{\partial^2 w}{\partial t^2} = 0 \tag{5}$$

Here D is the flexural rigidity, ρ is mass density, E is Young's modulus, h is the thickness of the shell, a is the radius of the cylindrical shell, and w is the normal displacement.

Let $w(x,t) = W(x)e^{j\omega t}$; here $W(x)$ is the amplitude of normal displacement and t is time. Then

$$\frac{d^4W}{dx^4} - k^4W = 0 \tag{6}$$

The solution of Equation (6) is

$$w(x,t) = \left(A_0 e^{-ikx} + B_0 e^{ikx} + C_0 e^{-kx} + D_0 e^{kx}\right) e^{j\omega t} \tag{7}$$

where A_0, B_0, C_0, D_0 are constant; k is the complex wave number and $k = k_1 + ik_2$. Given η the energy density for bending is derived based on normal displacement. For far field, the stationary solution of energy density is expressed as

$$\langle \bar{e} \rangle = \left(\frac{Eh^3}{24(1-\nu^2)} k_1^4 + \frac{1}{2}\rho h\omega^2\right)\left(|A_0|^2 e^{-\frac{\eta}{2}k_1 x} + |B_0|^2 e^{\frac{\eta}{2}k_1 x}\right) \tag{8}$$

Here ν is Poisson's ratio. The stationary power is expressed as

$$\bar{p} = 2\omega \frac{Eh^3}{12(1-\mu^2)} k^3 \left(|A_0|^2 e^{-\frac{\eta}{2}k_1 x} - |B_0|^2 e^{\frac{\eta}{2}k_1 x}\right) \tag{9}$$

According to (8) and (9), the relation of power to energy density can be expressed as

$$\frac{\partial \bar{p}}{\partial x} = -\frac{4C_f^2}{\eta\omega} \frac{\partial^2 \langle \bar{e} \rangle}{\partial x^2} \tag{10}$$

Here $c_f^4 = \omega^4 D / \left(\rho h\omega^2 - Eh/a^2\right)$. The steady state response, based on the principle of energy balance, becomes

$$\pi_{in} = \pi_{diss} + \nabla \bar{I} \tag{11}$$

For the hysteresis damping model [Zhang G., Vlahopoulos N. (2006); Vlahopoulos N.,Wang A.M. (2005); Wang A.M., Vlahopoulos N., Buehrle R. (2006)],

$$\bar{\pi}_{diss} = \eta\omega\bar{e} \tag{12}$$

The differential equation of energy density for a cylindrical shell can now be derived by considering a power balance at the steady state over a differential control volume of the shell. [Xie M. X., Chen H.L., Wu J.H. (2008)]

$$-\frac{4C_f^2}{\eta\omega} \frac{d^2 \langle \bar{e} \rangle}{dx^2} + \eta\omega \langle \bar{e} \rangle = \bar{\pi}_{in} \tag{13}$$

As illustrated in Equation (13), the energy density of the cylinder is axis-symmetric so we apply the axis-symmetric shell element to the dividing shell. The energy density of the shell can be obtained by solving Equation (13) numerically.

Let us consider an example. The cylindrical shell is made of aluminum with thickness $h = 0.01m$, length $l = 1m$ and radius $a = 0.5m$. Its properties are shown in Table 1. An input bending power density $\pi_{in} = 200J/m^2 \cdot s$ at a frequency f=1000 Hz is applied at one end of the cylinder. For the first case, Equation (13) is solved and the computed results are shown in Fig.1. For the other case, the energy finite element flat shell element model is comprised of 288 nodes, 270 rectangular flat shell elements, and 288 structural-structural joints. Power transfer coefficients are computed using the method developed by Langley and Heron [Langley R.S., Heron K.H. (1990)].

Table 1: Cylindrical shell properties

Mass density $\rho/(kgm^{-3})$	**Young's modulus** E/**Pa**	**Poisson's ratio** ν	**hysteresis damping factors** η
2700	7.1e11	0.33	0.01

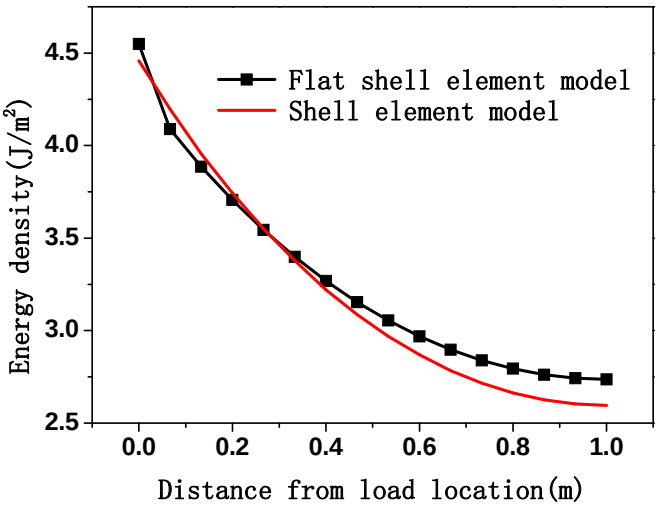

Figure 1: Energy density on a cylinder along the axis

The results of the flat shell element model are compared with the numerical solution of Equation (13) by an axis-symmetric shell element model. The energy density computed by the two methods is presented in Fig. 1. The largest error is at 1.0 m from load location along the cylinder's axis, where the energy density results of the flat shell element model is $2.75J/m^2$ and the energy density results of the axis-symmetric shell element model is $2.62J/m^2$, displaying an error of 5.57%. It can

be seen that good correlation is observed between the axis-symmetric shell element model analysis and the flat shell element model method, indicating that the flat shell element model is reasonable.

The approximate EFEA method can also be used for plate structures for dynamic response and structural-acoustic coupling problems. To further validate the accuracy of the approximate method, the structural-acoustic coupling characteristics of a simplified passenger vehicle model based on a model by Dong *et al.* [Dong J., Choi K.K., Wang A. M. (2005)] are computed and compared with results from Dong *et al*. The simplified passenger vehicle sketch is shown in Fig. 2. The passenger vehicle EFEA model is comprised of seven different structural panels made of 0.01 m thick aluminum. The acoustic space enclosed by the structural panels is filled with air. The model's properties are shown in Table 2. As the prism meshes used by Dong *et al.,* shown as Fig. 4(a), may affect the precision of results, a complete hexahedron mesh is used in the EFEA model shown in Fig. 3(a). A power density at a frequency of 2000Hz is applied at the four corners, similar to the input applied by Dong *et al.* The computed acoustic pressure is plotted in Fig. 3(b), while Fig. 4(b) illustrates the acoustic pressure at the boundary of the acoustic medium results from Dong *et al*. The good correlation between the two results again indicates that this paper's model is reliable.

Table 2: Properties of simplified passenger vehicle

Mass density of panel $\rho/(kgm^{-3})$	**Young's modulus of panel** E**/Pa**	**Poisson's ratio of panel** ν	**hysteresis damping factors of panel** η	**Mass density of acoustic medium** $\rho_0/(kgm^{-3})$	**wave speed of acoustic medium** $c_0/(ms^{-1})$	**hysteresis damping factors of acoustic medium** η_0
2700	7.1e11	0.33	0.01	1.02	343	0.001

4 EFEM analysis of a simplified aircraft cabin with the approximate method

In this section, EFEM analysis of an aircraft cabin using the approximate method is performed to optimize the cabin's noise and vibration performance and avoid damage of instruments inside the control cabin. A simplified aircraft cabin model comprised of a truncated conical shell structure with two end plates, as shown in Fig. 5, is constructed and studied for this purpose. The length of the truncated

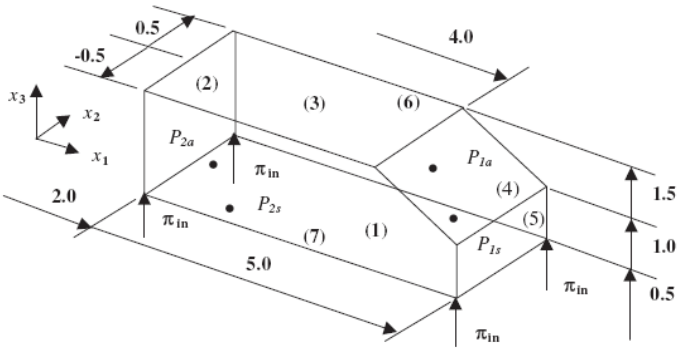

Figure 2: Simplified passenger vehicle model

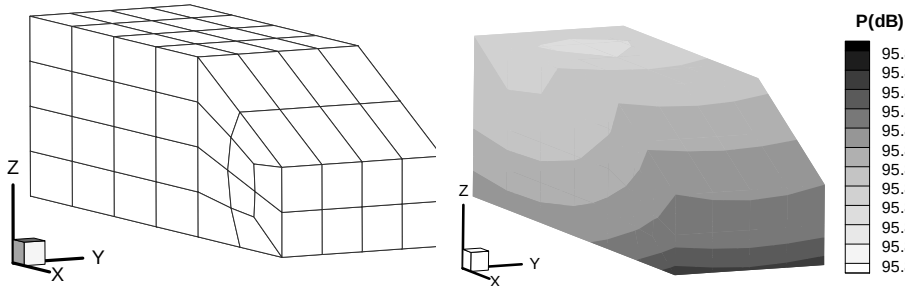

（a）EFEA model of simplified passenger vehicle **（b） Interior acoustic pressure distribution**

Figure 3: EFEA model and the results in current paper

conical shell is L, the thickness h and the radius at the ends are R1 and R2, respectively. The shell structure and two end plates have the same physical properties and the acoustic space enclosed by the truncated conical shell is filled with air. Fig. 6 shows the corresponding EFEM model for the aircraft cabin, comprised of 208 structural plate elements, 354 acoustics elements and 809 nodes, 48 structural-structural joints and 208 structural-acoustic joints.

4.1 EFEM analysis of aircraft cabin with imposed point load

A single point force of 50000N with a high frequency of 2088.1Hz is applied to the center of the small end plate of the truncated conical shell as excitation. The chosen frequency is a resonance frequency that the large section of the structure vibrates in the form of three pitch line radial motions. The structural-acoustic coupling prob-

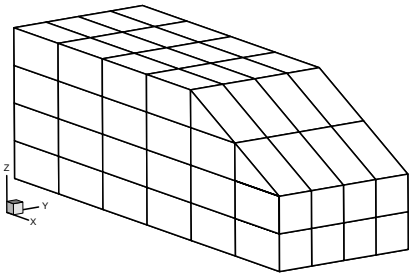

（a）EFEA model of simplified passenger vehicle in literature

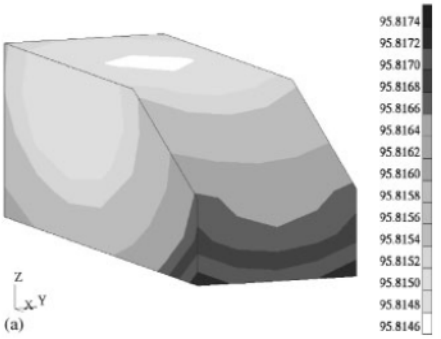

（b）Interior acoustic pressure distribution in literature

Figure 4: EFEA model and the results in literature [Dong J., Choi K.K., Wang A. M. (2005)]

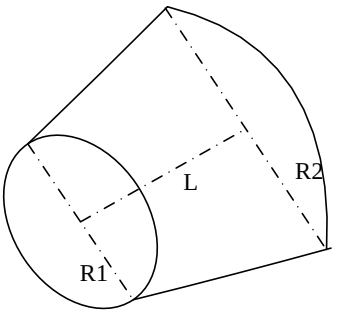

Figure 5: Dimensions of the aircraft cabin

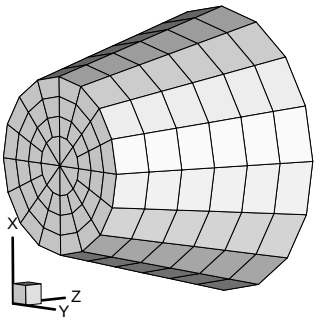

Figure 6: Energy Finite element model for the aircraft cabin

lem is solved using the approximate EFEM and acoustic energy is converted to the root mean square acoustic pressure with the approximation $p = c_0\sqrt{e\rho_0}$. The sound pressures are expressed in terms of decibel level with the acoustic pressure reference of $2 \times 10^{-5} Pa$. The computed results of interior acoustic pressure distribution in an acoustic medium at the x=0 symmetric plane, at the y=0 symmetric plane and the computed energy density distribution on the shell are shown in Fig. 7(a), Fig. 7(b) and Fig. 7(c), respectively.

The 50000 N input force is applied at point P, as shown Fig. 8, and the energy

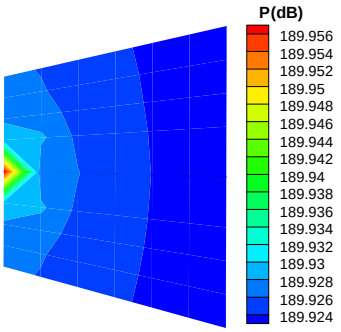

(a): Interior acoustic pressure at x=0 plane

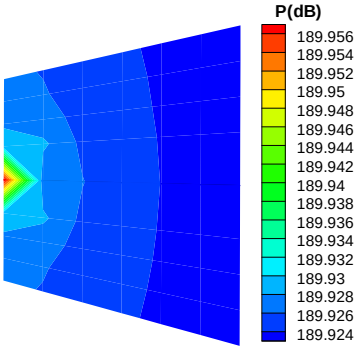

(b): Interior acoustic pressure at y=0 plane

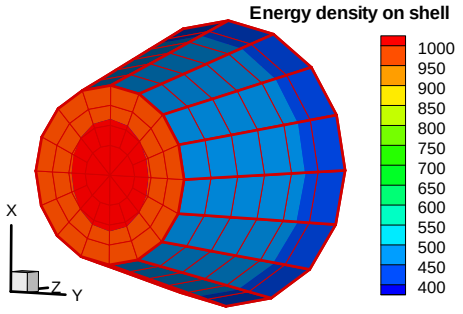

(c): Energy density distribution on the shell

Figure 7: Computed results for the truncated conical shell when a 2088.1 Hz load is imposed at the center of the small end plate

density distribution in the acoustic medium and in the shell are calculated. The acoustic pressure in terms of decibel level is plotted in Fig.8. Fig.8 (a) and Fig.8 (b) illustrate the acoustic pressure at the x=0 symmetric plane and y=0 symmetric plane of the acoustic medium, respectively. Fig.8(c) shows the distribution of energy density on the shell. In the figures showing acoustic pressure, red indicates high acoustic pressure while blue stands for low acoustic pressure.

These results show that energy density gradually decreased with increasing distance from imposed point load. However, the acoustic pressure of inside the cabin takes on an axis-symmetric distribution.

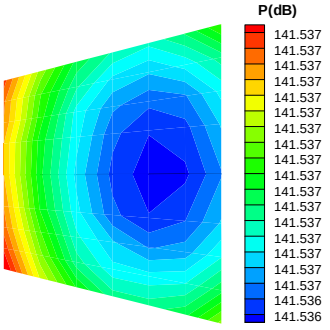

(a): Interior acoustic pressure at x=0 plane

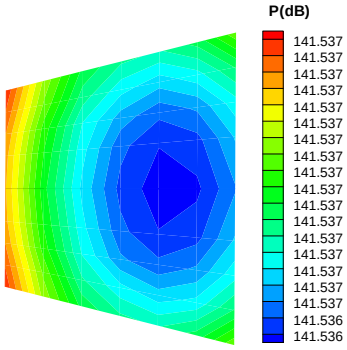

(b): Interior acoustic pressure at y=0 plane

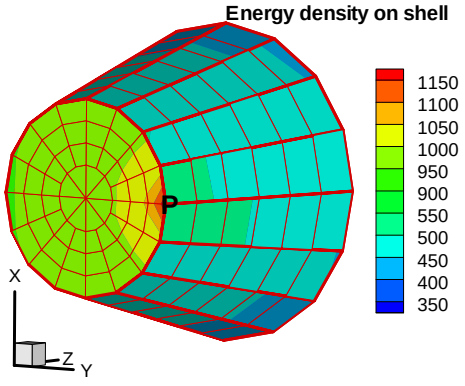

(c): Energy density distribution on the shell

Figure 8: Computed results at the truncated conical shell when a 2088.1 Hz load is imposed at point P

4.2 EFEM analysis of aircraft cabin with imposed fluctuating pressure load

4.2.1 Computing the fluctuating pressure load

The pressure exerted on a flying aircraft is the beat of the turbulent boundary layer and radiation sound pressure due to shell vibration. The radiation pressure is much smaller than the turbulent boundary layer pressure, so it is ignored here and the fluctuating turbulent boundary layer pressure distribution as an ideal source of stress is considered. The expression of the input power density due to the fluctuating

turbulent boundary layer pressure is [Yao D.Y., Wang Q.Z. (1995)]

$$p_{in} = \frac{2\pi^2 C_a^2 n_s(f)}{4\pi^2 f^2 \rho_s} \sigma_{rad} \left\langle p_a^2 \right\rangle \left\langle D(\Omega) \right\rangle \tag{14}$$

where C_a is acoustic wave speed, ρ_s is structural density, $n_s(f)$ is the modal density of the structure, σ_{rad} is radiation efficiency, p_a is acoustic pressure and $\langle D(\Omega) \rangle$ is directivity index.

For the truncated conical shell, modal density $n_s(f)$ is

$$n_s(f) = \begin{cases} 2.0 \left[\dfrac{R2\left(1-\frac{R1}{R2}\right)^{4/5}}{\pi h} \right] & f > \frac{C_l}{2\pi R1} \\ 1.31 \left[\dfrac{R2\left(1-\frac{R1}{R2}\right)^{3/4} (\omega R2)^{1/2}}{\pi h (C_l)^{1/2}} \right] & f < \frac{C_l}{2\pi R2} \end{cases} \tag{15}$$

Here C_l is the speed of the longitudinal wave.

In order to compute σ_{rad} in Equation (14), the truncated conical shell is simplified by the equivalent cylindrical shell according to the equivalence law such that: 1) the cylinder shell and the truncated conical shell are of the same material and the same thickness; 2) the cylindrical shell diameter is equal to the mean diameter of the large and small sections of the truncated conical shell; 3) the cylindrical shell length is the generatrix length of the truncated conic shell. Thus the radiation efficiency of the equivalent cylindrical shell is regarded as the radiation efficiency of the truncated conical shell.

When frequencies are higher than the ring frequency f_r of the equivalent cylindrical shell, the general effect of fluid loading on a cylindrical shell is similar to the fluid loading effect on a plate with the same area and same thickness as the cylindrical shell [Yao D.Y., Wang Q.Z. (1995)]. The expression of the ring frequency of a cylindrical shell is

$$f_r = \frac{C_l}{2\pi r_l} = \frac{\sqrt{E\rho/(1-\nu^2)}}{2\pi r_l} \tag{16}$$

Here r_l is the radius of the equivalent cylindrical shell.

Radiation efficiency of the structure is related to the coincidence frequency f_c, where the structural bending wave number coincides with the acoustic wave number [Zhang W.G., Wang A.M., Vlahopoulos N. (2003); Dong J., Choi K.K., Wang A.M. (2005)]. The expression of the coincidence frequency of the equivalent cylindrical shell is

$$f_c = \frac{C_a^2}{1.8 C_l h} \tag{17}$$

The radiation efficiency of the equivalent cylindrical shell can be expressed by

$$\sigma_{rad} = \begin{cases} \frac{\sqrt{3}}{2a}\left(\frac{f}{f_r}\right)^{\frac{3}{2}}\frac{f_r}{f_c} & f < f_r \\ \left[\frac{4\lambda_c}{\pi^2 A_c}(2\pi r_l + l_c)\arcsin\left(\frac{f}{f_c}\right)^{\frac{1}{2}}\right]\beta & f_r < f < f_c \\ \left(1-\frac{f_c}{f}\right)^{-\frac{1}{2}} = 2.38 & f > f_c \end{cases} \tag{18}$$

where A_c is the area of the equivalent cylindrical shell, λ_c is the wave length at coincidence frequency, l_c is the equivalent cylindrical shell length, $\beta = \sqrt{2}$ and $a = \begin{cases} 2.5\sqrt{\frac{f}{f_r}} & f < 0.5f_r \\ 0.36\frac{f}{f_r} & 0.5f_r < f < 0.8f_r \end{cases}$.

The value of $\langle p_a^2 \rangle$ in Equation (14) is obtained by wind tunnel test.

4.2.2 Aircraft cabin results with a fluid fluctuating pressure load

To investigate the energy flow in a wide band frequency range from 700–2000 Hz, the energy finite element model is solved at each center frequency of the one-third octave band (800 Hz, 1000 Hz, 1250 Hz, 1600 Hz, 2000 Hz). Energy density distributions from the aircraft cabin and acoustic pressure p_a due to the fluctuating pressure load are computed using EFEM under applied power flow in terms of Equation (14) and the acoustic energy computed is converted to the root mean square acoustic pressure. Consider the energy density variation at point B of the shell, shown in Fig 9. The energy density decreases with increasing frequency for a Mach number of 0.8 Ma and attack angle of 0 degrees. These results suggest that vibration is weak at high frequency.

When Mach number is 0.8 Ma and attack angle is 0 degrees, fluctuating pressure and energy density distribution of the aircraft cabin is expressed by Fig. 10(a) and Fig. 10(c), respectively. Fig. 10(b) shows the acoustic pressure distribution at the x=0 symmetric plane in the acoustic medium. Fig. 11 shows the results when the Mach number is 0.8 Ma and attack angle is 5 degrees. Fig. 12 is the results when Mach number is 1.15 Ma and attack angle is 0 degrees. Finally, Fig. 13 shows the results when Mach number is 1.15 Ma and when attack angle is 5 degrees.

The results in Figures 10–13 show that:

1. In each case, the variation of acoustic pressure in the acoustic medium enclosed by the cabin is very small. Energy propagation and decay still makes the acoustic pressure diminish from the boundary to the centre.

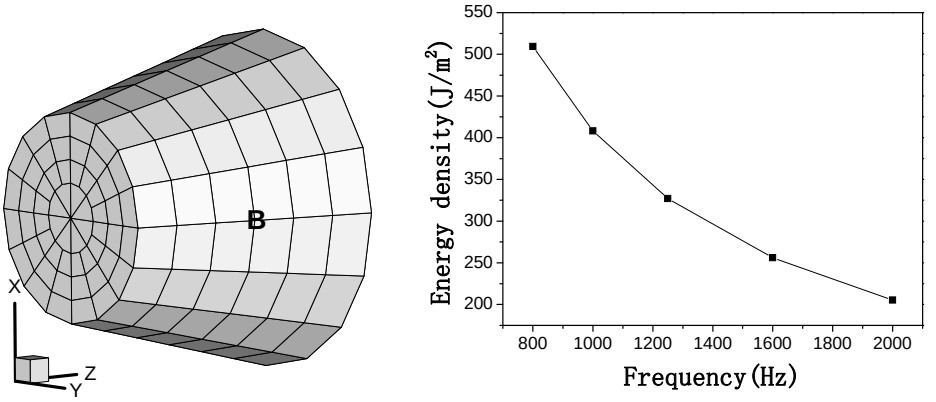

(a) (b)

Figure 9: (a): Location of point B; (b): Variation of energy density at point B against the frequency of load

2. When the attack angle is 0 degrees, the same cross-section of cabin has the same approximate energy density because the distribution of fluid pressure is axis-symmetric. When the attack angle is 5 degrees, the distribution of fluid pressure and the distribution of energy density in the cabin is not axis-symmetric and the closer to the load location the larger the energy density. This suggests that the load distribution is the factor affecting the energy density distribution on the cabin.

3. The value of energy density on the cabin and the acoustic pressure are increasing dramatically with Mach number increasing from 0.8 to 1.15 Ma. It appears that the vibration amplitude of the cabin is intensively dependent on Mach number.

4. No matter the value of attacking angle, the energy density at the smaller diameter end is larger than the energy density at the end with large diameter because of the fluid direction.

5 Summary

An approach for computing aircraft cabin structural-acoustic characteristics using EFEM is developed and presented. The approach was first validated using a simple cylindrical shell structure for numerical testing and the results demonstrate an

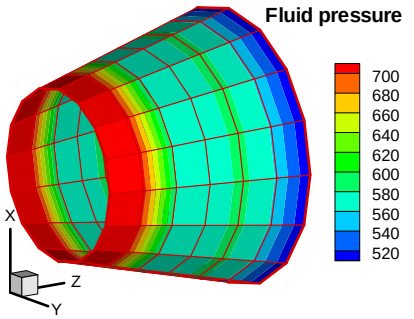

(a): Turbulent boundary layer pressure

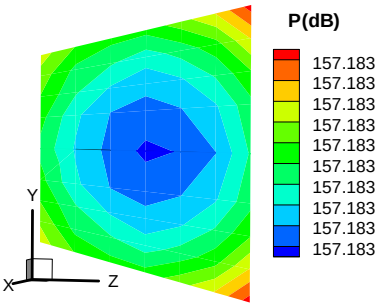

(b): Distribution of interior acoustic pressure at the x=0 symmetric plane for the aircraft cabin

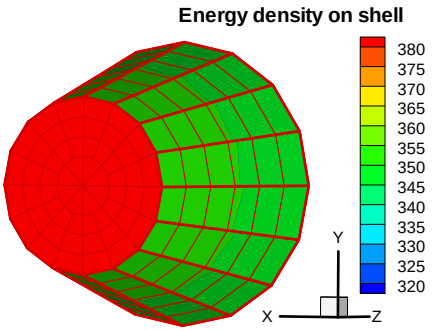

(c): Distribution of energy density on the shell

Figure 10: (color online) Simulation results. (0.8 Ma, Attack angle is 0 degrees)

excellent agreement with EFEM results when applied to axis-symmetric shell elements. A second numerical example using a simple passenger vehicle was performed with EFEM and the results agreed with those reported in literature. To compute the aircraft cabin structural-acoustic characteristics, a wind tunnel test first provided the fluid pressure of an aircraft cabin at four different flying conditions. The structural-acoustic characteristics of the aircraft cabin under different flying conditions were then computed using the method presented in this paper. The cabin energy density and acoustic pressure inside the cabin at different attack angles and different Mach numbers were computed and analyzed.

The aim of this research is to propose a method to solve the structural-acoustic coupling problem of an aircraft cabin. The results of this study may lead to the devel-

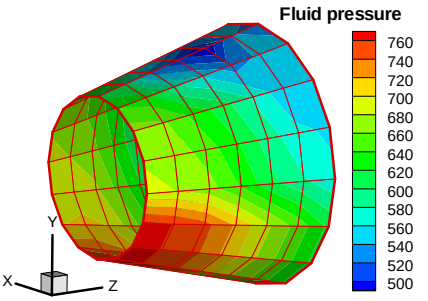

(a): Turbulent boundary layer pressure

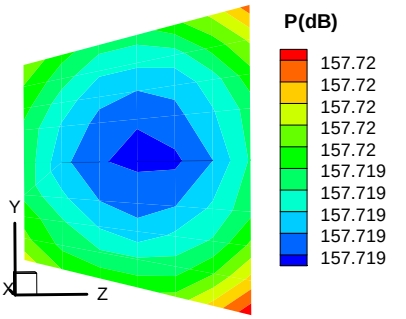

(b): Distribution of interior acoustic pressure at the x=0 symmetric plane for the aircraft cabin

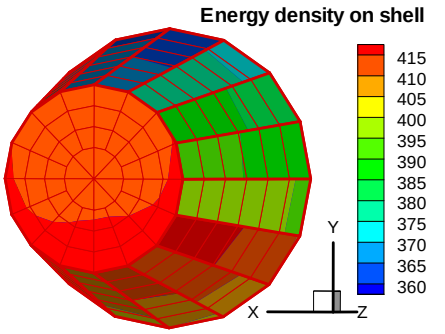

(c): Distribution of energy density on the shell

Figure 11: (color online) Simulation results. (0.8 Ma, Attack angle is 5 degrees)

opment of effective methods for solving the structural-acoustics coupling problems for other shell structures. An important direction for further work might be to study complex structures such as rib and non-axisymmetric structures.

Acknowledgement: The authors gratefully acknowledge Mr. Gao C from Northwestern Polytechnic University for providing experiment data. The author also thanks Ms Wang N from Northwestern Polytechnic University for helpful discussion and advice.

References

Bernhard R. J. ; Huff J. E. (1999): Structural-acoustic design at high frequency using the energy finite element method. *Journal of vibration, Acoustics Stress and Reliability,* vol. 220, pp.135-154.

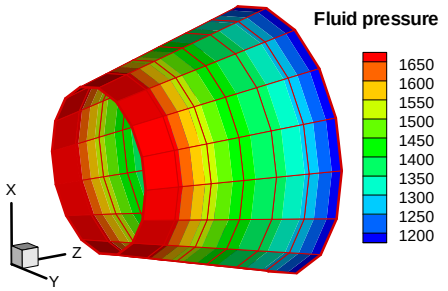

(a): Turbulent boundary layer pressure

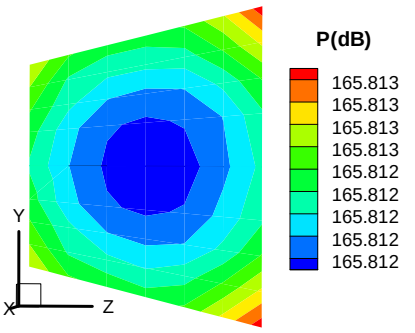

(b): Distribution of interior acoustic pressure at the x=0 symmetric plane for the aircraft cabin

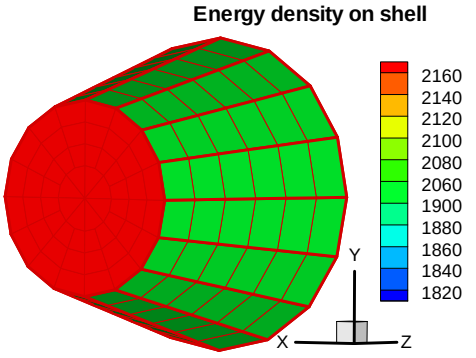

(c): Distribution of energy density on the shell

Figure 12: (color online) Simulation results. (1.15 Ma, Attack angle is 0 degrees)

Bitsie F. (1996): The structural-acoustics energy finite element method and energy boundary element method. *Ph. D Thesis,* Purdue University.

Bouthier O. M.; Bernhard R. J. (1995): Simple models of energetics of transversely vibrating plates. *Journal of sound and vibration*, vol. 182(1), pp.149-164.

Brancati A.; Aliabadi M. H.; Benedetti I. (2009): Hierarchical Adaptive Cross Approximation GMRES Technique for Solution of Acoustic Problems Using the Boundary Element Method. *CMES: Computer Modeling in Engineering & Sciences,* vol. 43(2), pp. 149-172

Dong J; Choi K.K.; Wang A. M. (2005): Parametric design sensitivity analysis of high-frequency structural-acoustic problems using energy finite element method.

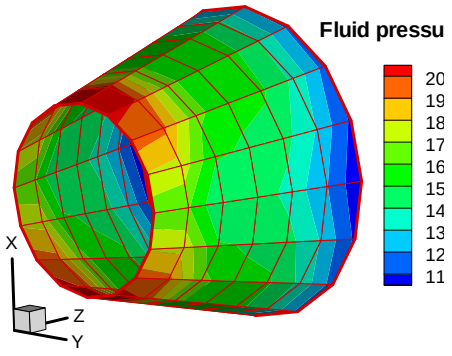

(a): Turbulent boundary layer pressure

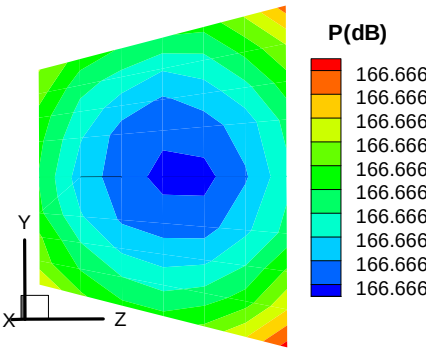

(b): Distribution of interior acoustic pressure at the x=0 symmetric plane for the aircraft cabin

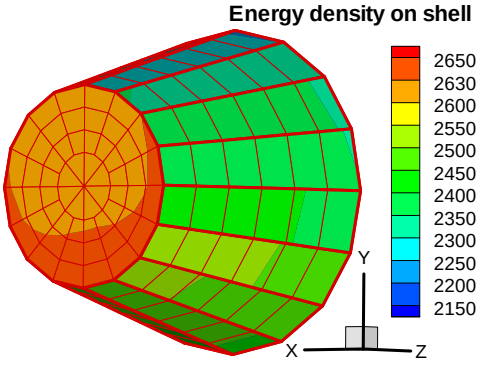

(c): Distribution of energy density on the shell

Figure 13: (color online) Simulation results. (1.15 Ma, Attack angle is 5 degrees)

International journal for numerical method in engineering, vol. 62, pp. 83-121.

He F. B.; Shen Y. P. (2008): Theory of plate and shell. XI'AN Jiaotong University Press, 1993.

Langley R. S.; Heron K. H. (1990): Elastic wave transmission through plate/beam junctions. *Journal of sound and vibration*, 143(2):241-253.

Moravaeji S. J. (2008): Modeling of trim panels in the energy finite element analysis, in Naval Architecture and Marine Engineering. *The University of Michigan: Ann Arbor.*

Nefske D. J.; Sung S. H. (1989): Power flow finite element analysis of dynamic systems: basic theory and applications to beams. *ASME Transaction, Journal of Vibration, Acoustics Stress and Reliability in design,* vol. 111(1), pp. 94-100.

Raymond F.; Leo B.; Layton G.; David B. (2006): Energy finite energy analysis for shipboard noise. *J. Acoust. Soc. Am.*, 120(5): 3287, Pt. 2, Fourth Joint Meeting: ASA and ASJ, November.

Vlahopoulos N ; Wang A.M. (2005): An EFEM formulation for computing the structural response of complex structures. *American Society of Mechanical Engineers, Noise Control and Acoustics Division (Publication)* NCA, vol. 32, pp. 109-114.

Wang A.M.; Vlahopoulos N.; Buehrle R. (2006): Energy finite-element analysis of the NASA aluminum testbed cylinder. *J. Acoust. Soc. Am.*, vol. 119(5), pp.3389, Pt. 2.

Wu K.C.; Vlahopoulos N. (2004): Vibratory response of surface ships predicted by energy finite element approach. *J. Acoust. Soc. Am.*, vol. 116(4): 2569, Pt. 2, October.

Wu K.C.; Vlahopoulos N. (2006): Recent developments and applications of energy finite- element analysis. *J. Acoust. Soc. Am.*, vol. 120(5), pp. 3343 Pt. 2, November, Fourth Joint Meeting: ASA and ASJ.

Xie M. X., Chen H. L.; Wu J. H. (2008): Energy finite element analysis to high-frequency bending vibration in cylindrical shell. *Journal of xi'an Jiaotong university*, vol. 42(9), pp.1113-1116.

Yan X. Y. (2008): Energy finite element analysis development for high frequency vibration analysis if composite structures, in Naval Architecture and Marine Engineering. *The University of Michigan: Ann Arbor.*

Yao D.Y.; Wang Q.Z. (1995): Statistical energy analysis: Theory and applications. Beijing Institute of Technology Press.

Zhang W. G. (2003): energy finite element method for vibration analysis of stiffened plates under fluid loading, in Naval Architecture and Marine Engineering. *The University of Michigan: Ann Arbor.*

Zhang W. G.; Raveendra S.T. (2008): Application of energy finite element method for high frequency vibro-acoustic analysis, in Noise control. *INCE: Dearborn, Michigan.* pp. 1453-1463.

Zhang G.; Vlahopoulos N. (2006): Combining an energy boundary element analysis with an energy finite element analysis for computing airborne noise inside a flexible structure due to an exterior acoustic source. *J Acoust Soc Am*, 119(5), pp.3418, Pt. 2.

Zhang W.G.; Wang A.M.; Vlahopoulos N. (2002): An alternative energy finite element formulation based on incoherent orthogonal waves and its validation for marine structures. *Finite elements in analysis and design*, vol. 38(12) , pp.1095-1113.

Zhang W.G.; Wang A.M.; Vlahopoulos N. (2003): High-frequency vibration analysis of thin elastic plate under heavy fluid loading by an energy finite element formulation. *Journal of sound and vibration*, vol. 263(1) , pp. 21-46.